Comparison of Real-Time Monitoring of Copolymer Formation and Composition by NMR, FTIR, and Numerical Simulation

Seán J. Martin,[†] Vincent J. McBrierty,*[,†] and Dean C. Douglass[‡]

Physics Department, Trinity College, Dublin 2, Ireland; and 120 Dyckman Place, Basking Ridge, New Jersey 07920

Received April 13, 2001; Revised Manuscript Received August 23, 2001

ABSTRACT: This paper reports on the use of high resolution NMR to profile the curing dynamics in real time of two monomer mixes, one predominantly HEMA and the other a HEMA/NVP/TBE comonomer. FTIR data on the same materials permit examination of the complementarity of NMR and FTIR in probing curing dynamics. The observed responses are compared with simulations generated by a new program which is applicable to an N-component monomer mix, using published reactivity ratios for NVP and HEMA and those of a reasonable analogue for TBE. The ability to monitor NMR chemical shift and line shapes as curing proceeds provides additional insight into the curing dynamics. Differences in the curing profiles observed in the two experimental approaches are rationalized in terms of their relative sensitivities to short and longer range effects in the curing monomer. Agreement among data types is good whereas details relating to relative sensitivities are in part tentative and merit more detailed investigation.

The curing profile of the constituent monomers in a composite monomer mixture establishes the molecular composition of the resulting copolymer. This generic information, in turn, clarifies the relationship between macroscopic properties and microscopic behavior of the cured system and, conversely, facilitates the tailoring of new composite polymers to meet specific applications. With this in mind, a systematic study on the curing dynamics of selected monomer composites has been carried out along three distinct, but related, lines. The first and primary goal was to demonstrate and validate the way in which high resolution NMR probed the curing dynamics of individual monomer constituents in a composite system in real time. Second, FTIR data on the same monomer composites provided interesting insight into the complementarity of the two experimental approaches. Third, the numerical simulation of oligomer concentrations throughout the course of polymerization of an N-component monomer composite (N = 2, 3, 4, ...) generated additional perspective. The novelty of this simulation is the recognition that the kinetic equations, as usually expressed, with modest algebra can be converted to a form that is then dealt with by a standard, commercially available, numerical package. Owing to the absence of information about radical kinetics in the underlying kinetic relations, the simulation describes compositions as a function of degree of polymerization; it cannot provide the time dependence of the curing process per se.[1,2]

The following monomer constituents with known or readily deduced reactivity ratios (or $Q-e$ values) were used to explore and validate the NMR approach: *N*-vinyl-2-pyrrolidone (NVP), hydroxyethyl methacrylate (HEMA) and the modulus modifier 4- or 5-*tert*-butyl-2-hydroxycyclohexyl methacrylate (TBE). These monomers are both scientifically and commercially important because of their widespread use in the manufacture of hydrogel contact lenses.[3−6]

A significant body of data has been compiled on polymerization kinetics by assessing the amount of polymer formed in a series of sequential experiments whereby the curing process, usually for monomers in dilute solution, is arrested after specified periods of time.[7−9] Standard kinetic equations with reactivity ratios of pairs of monomers as disposable parameters are then used to extrapolate curing behavior over the complete curing cycle. More recently the advent of FTIR spectrometers with improved spectral acquisition speeds and signal-to-noise ratios, superior UV light sources, and increasingly sophisticated data processing techniques, permitted quantitative studies of photoinitiated or thermally induced polymerization in real time.[10,11] In this approach curing profiles are constructed from the diminishing intensity of specific absorbance bands that are sensitive to polymerization as curing proceeds, primarily the fractional conversion of carbon−carbon double bonds. Problems often arise due to poor resolution owing to overlapping bands in the spectrum and the need to monitor internal reference bands to obviate further complications due to changes in sample thickness arising out of shrinkage or thermal expansion.

An alternative to FTIR, based on the site-specificity of high resolution NMR, provides an appreciably more informative approach and forms the central focus of this study. The intensity, shape, and position (chemical shift) of labeled peaks in the NMR spectrum contain valuable site-specific information on molecular motion and chemical environment.[12] This has been demonstrated for a range of monomer composites investigated in our laboratory where liquid NMR spectra include resolved peaks that uniquely label each of the monomer constituents.[3] These spectral peaks can be monitored continuously as curing proceeds from the liquid state via a gel phase toward the fully cured solid polymer. Curing profiles are generated from the intensities of NMR spectral lines that label each constituent monomer while details of curing dynamics at the molecular level are encoded in their chemical shifts and line shapes.

The observed decrease in peak intensity with curing can be explained as follows. The transformation from

* To whom correspondence should be addressed.
[†] Trinity College.
[‡] 120 Dyckman Place.

10.1021/ma010645z CCC: $20.00
Published on Web 11/22/2001

liquid monomer to solid polymer induces line broadening and when all or part of the line exceeds the relatively narrow bandwidth of the liquids probe (typically 4 kHz), it collapses into the baseline. With the possible exception of very short oligomers, only the liquidlike remnant monomer contributes to the residual spectral peak. Temporal information on the curing dynamics is thus encoded in the diminishing intensity of the relevant spectral peaks as curing proceeds. Note too that the sensitivity of NMR spectra to the presence of unpaired electrons offers the possibility of at least cursory examination of free radical activity in the monomer system as it progressively transforms into the solid polymer.

Both the FTIR and NMR methods rely on the availability of pulsed lasers that can deliver precisely defined light energy within specified time periods thereby permitting controlled experiments in a way that was not possible heretofore with the more traditional UV light sources. Experiments of this nature have, for example, allowed the optimization of curing parameters. Moreover, access to pulsed UV irradiation whereby the amount of cured monomer can be monitored while the laser is pulsed on and off for selected periods of time affords an alternative route to information on curing dynamics.[10]

Experimental Procedure

Sample Characterization. Of the two monomer compositions examined, Sample A was exclusively HEMA with trace amounts of the cross-linker ethylene glycol dimethacrylate (EGDMA) and the initiator benzoin methyl ether (BME). Sample B contained NVP (44.6 wt %)/HEMA (32 wt %)/TBE (8 wt %) with trace amounts of the cross-linkers hydroxyethyl methacrylate vinyl carbonate (HEMA VC) and EGDMA. In both cases, 15 wt % glycerol, a nonreactive diluent and processing aid, was initially present in the monomer but was later washed out of the cured polymer to mimic the final hydration step in the manufacture of contact lenses. Darocur 1173 (α-α-dimethyl-α-hydroxyacetophenone) was used as photo initiator. The source and characterization of the various reagents are listed elsewhere.[3,6] In all curing experiments, the liquid monomer was degassed by pumping on it for a period of 30 min before its transfer to the NMR tube or FTIR sample holder prior to data acquisition.

Ultraviolet−Visible Spectroscopy. UV absorption data were recorded on a Shimadzu UV-1601 PC double beam grating spectrophotometer linked to a 486 PC with UVPC spectroscopy software version 3.7 operating within the Microsoft Windows 3.1 protocol. These data identified the usable range of UV radiation wavelengths as 300−380 nm. Below ca. 300 nm, high absorption limits sample penetration thereby confining polymerization to the sample surface region. Above 380 nm, absorption is too low to effect efficient bulk polymerization of the monomer.

FTIR Data Acquisition. Infrared spectra of the composite monomer mixtures and their individual constituents were recorded between 4800 and 400 cm^{-1} on a Nicolet 510-P FTIR spectrometer with a spectral resolution of 1 cm^{-1} using a horizontal attenuated total reflectance (ATR) sampling accessory. A detailed assignment of the functional groups responsible for each absorbance in the spectra identified those bands that were sensitive to the progression of polymerization and those that could be used as internal references. To effect UV irradiation in the in situ FTIR curing experiments, a Specac variable-temperature cell unit was modified by inserting an airtight port into the side wall of the cell to support a UV grade fiber optic bundle carrying light pulses from a UV VSL-337 nitrogen laser operating at 337 nm. The sample holder was in the form of two shaped NaCl plates separated by a teflon spacer 0.1 mm thick. Degassed monomer was introduced into the cell via injection ports in the top plate which also included a suitable receptacle for a thermocouple. The loaded sample holder was then placed in the variable temperature cell and maintained in an atmosphere of dry nitrogen gas.

NMR Data Acquisition. High-resolution liquid spectra of the monomer mixtures and their constituents were recorded on a Bruker MSL 300 spectrometer operating at 300.13 and 75.47 MHz for protons and carbons respectively using a suitably modified CIDNP probe, as described below. A specified amount of the degassed sample (typically 0.25 g by weight) was transferred under an atmosphere of dry N_2 gas to an NMR sample tube and sealed. In situ UV curing was achieved with laser light delivered to the sample in the modified probe. The UV laser delivered pulses of radiation via a UV grade fiber-optic bundle 3 mm in diameter which was connected to the probe's base. Pulses of 3 ns duration were delivered at a pulse rate of 20 Hz, generating a maximum power output of 3 mW, equivalent to 2.64 mW average power output. A coupling stage interfaced the fiber-optic bundle to a quartz rod located alongside and parallel to the sample tube. The top face of the rod was angled at 45° to the vertical in order to direct light toward the sample through a vertical collimator slit in a teflon sheath encasing the top of the rod. About ca. 7% of the average power output of the laser, corresponding to an average intensity of ca.0.25 mW cm^{-2}, was delivered to the sample in the probe of which ca. 12% ultimately reached the monomer inside the NMR tube. This corresponded to an average intensity of 0.03 mW cm^{-2}. The conventional Bruker temperature measurement facility was used for in situ thermal curing to an accuracy of ±1.0 K.

^1H spectra with 16 K data points zero-filled to 32 K points were compiled with a standard pulse sequence employing quadrature detection, a pulse length of 3 μs, a 5 s delay between data acquisition cycles, and a sample spinning rate on the order of 5 Hz.[12,13] In the event that ^{13}C spectra are needed to obtain improved spectral resolution, albeit with the penalty of significantly longer spectral acquisition times, off-resonance, inverse-gated, proton-decoupling combined with the WALTZ16 pulse sequence can be employed.[14]

In real-time curing experiments, proton free induction decays (FIDs) were stored approximately every 30 s throughout the curing cycle, from which selected spectra were Fourier transformed, phase corrected, and baseline adjusted. Component peak intensities and peak areas were recorded as a function of curing time.

Results and Discussion

Computer Simulation of Curing Dynamics. Walling and Briggs[15] extended the work of Alfrey and Goldfinger[16] on two-component kinetics to differential forms for the kinetics of multicomponent monomer mixes. This early work introduced the astute observation that elimination of time as a variable from the chemical kinetic equations via the assumption that all radical concentrations rapidly attain a quasi-steady state, provides ratios of differentials of monomer concentration solely as a function of monomer concentrations. Solution of these coupled differential forms yields the concentrations of monomers and instantaneous composition as a function of the degree of polymerization. Alfrey and Price[17] introduced the $Q-e$ scheme for an accurate general form to represent the relative, binary kinetic parameters obtained experimentally. Valvasorri and Sartori[1] have generated a convenient representation of the multicomponent differential relations in terms of the $Q-e$ parameters; it is this representation which is used as the starting point of the current numerical simulation of the radical copolymerization process.

The differential forms are always first order in *differential* monomer concentration, but they are in

general nonlinear in monomer concentrations; only numerical solutions can be expected to be practical. Readily available numerical routines for solution of differential equations assume that the input system of equations has the form of first-order differentials with respect to an independent variable. In the problem at hand the true independent variable in an experimental sense has been eliminated and so must be replaced by something else in order to use the standard numerical packages. The degree of polymerization, θ, is the logical choice as the replacement. However, since θ depends on concentrations, it may not be considered independent unless one monomer concentration is eliminated from the kinetic equations. This elimination is readily carried out algebraically by use of the definition of the degree of polymerization,

$$\theta = 1 - \sum_{i=1}^{n} [C_i]$$

where concentrations are expressed as mole fractions. This step is described in detail in the Appendix. Because the differential equations are nonlinear and rate constants can differ by orders of magnitude, these equations have the potential of becoming stiff in some concentration ranges and the choice of concentration variable could in principle have an effect on the degree of stiffness that can develop. However, no problem of this nature has been observed in our use of this technique. If such stiffness were to develop, it would become evident in the operation of the Runge−Kutta algorithm used herein and steps to correct the problem can be made, steps such as a differing choice of concentration for elimination or use of an algorithm developed for stiff equations.[18] Indeed, the fifth-order Runge−Kutta algorithm with adaptive step size used here[19] has a reputation of being satisfactory for moderately stiff equations. Application of the Runge−Kutta algorithm to copolymerization in order to produce plots of instantaneous mole fraction concentrations in the copolymer, as well as the directly calculated monomer concentrations, requires but one modification of the standard package, namely, storage of the rates, $d[C_i]/d\theta$. The instantaneous mole fractions in the copolymer are given directly by ratios of these rates.[20] The curing profiles or, if required, the instantaneous composition of the cured polymer at any given degree of conversion, have been calculated for composites with up to six monomer components on a 33 MHz NCR PC with an Intel 486 processor using a PowerBasic compiler.[21] No instabilities were encountered and calculation, storage, and display of results generally required less than 1 s.

FTIR Data and Analysis. The use of FTIR to monitor the curing profile of the constituent monomers in a composite sample relies on the prerequisite characterization of both component and composite FTIR spectra, in particular, the identification of suitable curing-sensitive and internal reference bands. Data for samples A and B and their primary constituents are shown in Figure 1, parts a−c, and summarized in Table 1. From these data, it is evident that this approach can be used to construct the curing profile of HEMA in sample A since bands that are sensitive to the curing process are reasonably well resolved. This is not the case however with sample B since the TBE bands of interest overlap those of HEMA and NVP with two consequences: First, access to the curing profile of TBE is precluded because of poor band resolution and because of its low concentration. Second, the concomitantly minor contribution of TBE to the overlapping HEMA and NVP bands implies that a reasonably good approximation of the curing profile for HEMA and NVP can be constructed without further correction.

Figure 2 presents data for sample B in the form of plots of remnant NVP and HEMA monomer as a function of curing time which confirm the very different curing dynamics of the two major constituents. The curing rate in NVP is low over the first ca. 1000 s, then increases quite markedly up to 2500 s before decreasing again in an asymptotic approach toward completion. Note, however, that complete cure is not achieved in this and subsequent curing cycles reported in the paper; extractables amounting to no more than a few percent remain. The more rapid curing profile of HEMA exhibits inflection points at ca. 400 and 700 s and the final low rate of cure sets in at ca. 1500 s, no doubt reflecting the complex curing dynamics of the multicomponent system with the added dimension of diffusion-controlled effects.

The data are presented in an alternative form in Figure 3 which plots the mole fractions of monomer components against degree of conversion. Model simulations based on the parameters listed in Table 2[6,8] are in excellent agreement with the experimental data. In these simulations the actual mole fractions of NVP and HEMA are adjusted upward to 0.62 and 0.38, respectively because the unresolved TBE component was ignored in the calculation. As will be evident in the NMR data, TBE cures at a rate that is intermediate between HEMA and NVP which would contribute to the slight overestimate of NVP curing rate and underestimate of HEMA curing rate in the model calculation.

At first sight, the C═C band at 1638 cm^{-1} in sample B offers a route to the curing profile of the composite as a whole but, unfortunately, this strong band is readily saturated, even for very thin monomer specimens. Additionally, poor resolution between this band and the even stronger and broader neighboring C═O band at 1717 cm^{-1} collectively imposes severe limitations on the accuracy of these measurements.

NMR Data and Analysis. Proton liquid NMR spectra for sample A over the curing cycle are shown in Figure 4 in the form of a stacked plot. Either of the peaks labeled e and f, identified earlier,[3] is a suitable candidate for probing the curing of HEMA in real time. Recall that spectra were recorded and stored approximately every 30 s throughout the curing cycle from which peak intensities were computed as a function of irradiation time. Curing profiles constructed from these intensity data, in this case with temperature as an additional disposable parameter, are shown in Figure 5. As expected, the curing rate progressively increases with increase in temperature from 293 to 333 K.

Data for sample A, which is a single component monomer, are only of passing interest but for the fact that they validate the methodology and instill confidence in the overall efficacy of the NMR approach. This view is further reinforced by the close agreement between the experimental results and theoretical model predictions, discussed below.

NMR data for sample B, on the other hand, are significantly more interesting in their ability to delineate the curing profile of each of the three major monomer constituents in the composite system. The

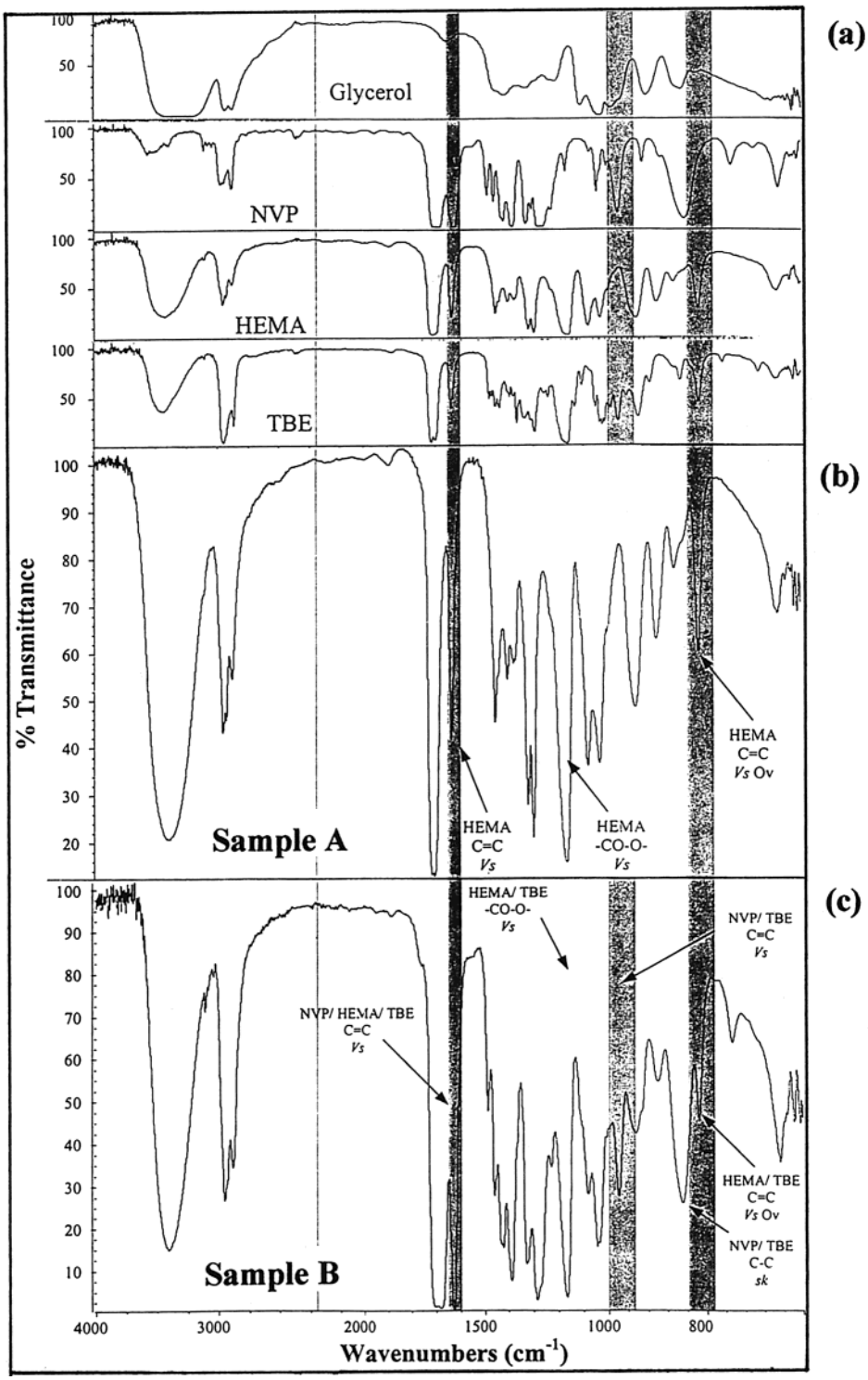

Figure 1. FTIR spectra of samples A and B along with their main constituents. The shaded areas highlight curing sensitive bands. Internal reference bands are also indicated.

Table 1. Relevant FTIR Curing-Sensitive and Internal Reference Bands in the Monomer Composites (See Text)

type of band	band	position (cm^{-1})	host monomers		
			HEMA	NVP	TBE
curing-sensitive	C=C	ca. 1638	√	√	√
		ca. 815	√		√
		ca. 981		√	√
internal reference	−CO−O−	ca. 1163	√		√
	−C−C−	ca. 850		√	√

stacked plot, recorded over a curing time of 4000 s, clearly shows the progressive decay of peaks representative of NVP, HEMA and TBE as curing proceeds (Figure 6). The corresponding curing profiles, normalized to 100% at $t = 0$, are furnished in Figure 7. Qualitatively, the data confirm earlier findings which indicate that the curing rate in NVP accelerates once curing in HEMA and TBE approaches completion.[20] Though not readily apparent in Figure 7, persistent oscillatory behavior is observed in the curing profile of NVP over the initial ca.700 s of UV irradiation. Simulated profiles based on the parameters listed in Table 2 are furnished in Figure 8. Because $Q-e$ values for TBE

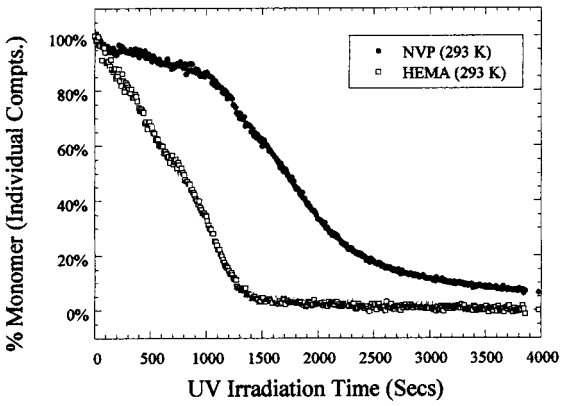

Figure 2. Curing profiles of NVP and HEMA in sample B as a function of curing time determined from the intensity vs UV irradiation time of the 981 and 815 cm^{-1} FTIR spectral bands, respectively.

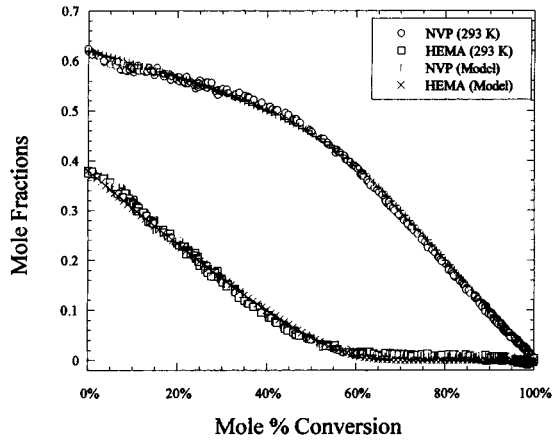

Figure 3. Comparison of the FTIR experimental UV curing profile of sample B with the simulated curing profile based on a two-component model (see text): NVP, $Q = 0.14$, $e = -1.14$; HEMA, $Q = 0.80$, $e = 0.20$.

Table 2. $Q-e$ Values and Mole Fractions of the Monomer Constituents in Sample B Used in the Theoretical Simulations in Figures 3 and 8

monomer	mole fraction in monomer mix	Q	e
NVP	0.59	0.14	−1.14
HEMA	0.36	0.80	0.20
TBE	0.05	0.88	0.24

were unavailable, data for ethylene glycol dimethacrylate were used as a reasonable alternative. A number of preliminary conclusions can be drawn from these results:

Model calculations are in agreement with earlier two- and three-component simulations reported in the literature.[20]

The simulation model predicts about 5% greater conversion of NVP monomer than is experimentally detected over the first half of the curing cycle. This can be due to a number of factors; an overestimation of NMR spectral peak intensities; an underestimation of the amount of NVP monomer in the composite; or inaccurate $Q-e$ values. Differences no doubt are also technique-related in view of the significantly better agreement achieved between the model simulations and the FTIR data furnished in Figure 3 (vide infra).

A better fit with the experimental data in Figure 8 could be achieved with a downward shift in HEMA monomer content which is in accord with the speculated increase in NVP content proposed above.

The observed retardation in the curing rate at the degree of conversion of ca.0.35 is consistent with the onset of diffusion-controlled curing which is not accommodated in the model calculation.

These predominantly macroscopic features of the curing dynamics are now examined further in terms of the detailed information contained in the spectral line shapes which are influenced, among other things, by the free radicals produced by UV irradiation.[12]

Line shape and Chemical Shift Analysis. Line shape and chemical shift analysis provide a more microscopic picture of events at a molecular level. Figure 9 portrays the superimposed line shapes of the three major monomer constituents in sample B recorded as a function of curing time. To facilitate interpretation of the rather convoluted dependence of the line shapes on curing, the data are recast in the form of chemical shifts of resolved subpeaks plotted as a function of curing time (Figures 10−12). Also reproduced in the plots are the curing profiles (dashed lines) along with the spectral line widths (ΔB) recorded as a function of curing time. The oscillatory dependence of ΔB on curing time in the initial phase of cure is included as an insert in each of the diagrams.

The following analysis of the response of the most complex NVP component provides an interpretational framework which also accounts for the responses of HEMA and TBE components.

There are a number of potential contributors to the observed oscillations in the initial part of the curing profile and the line width ΔB for $t \leq 700$ s: First is the dynamics of free radical generation and their subsequent influence on the NMR line shape before being masked by the onset of larger scale effects due to the formation of oligomers of increasing length; second is the response to cure of superimposed constituent subpeaks in the recorded NMR spectral lines, each exhibiting noticeably different chemical shift behavior with the progress of inhomogeneous polymerization (see below); third is the degree of uniformity of sample irradiation; and, fourth, possible effects associated with the UV laser pulse rate of 20 Hz. A detailed analysis of these factors must await further study involving a more focused series of experiments confined to the initial phase of the curing cycle.

The coexistence of broad and narrow peaks for curing times in excess of 1300 s provides direct evidence of inhomogeneous cure in the composite monomer. The extent to which this is an inherent feature of the curing dynamics or is due to experimental factors such as nonuniform UV irradiation of the sample will also be the subject of further study.

The decrease in ΔB and the concomitant increase in chemical shift at 85−90% conversion denotes the progressively dominant influence of remnant monomer and/or short oligomers which persist even to very long curing times. At this stage of almost complete polymerization, it is recalled that the contribution from the fully cured polymer far exceeds the bandwidth of the liquids probe and has been subsumed into the baseline.

An analysis of the overall pattern of chemical shift, line width, and remnant monomer as a function of curing time is bound up with inherent differences in the FTIR and NMR approach at the molecular level, as discussed below.

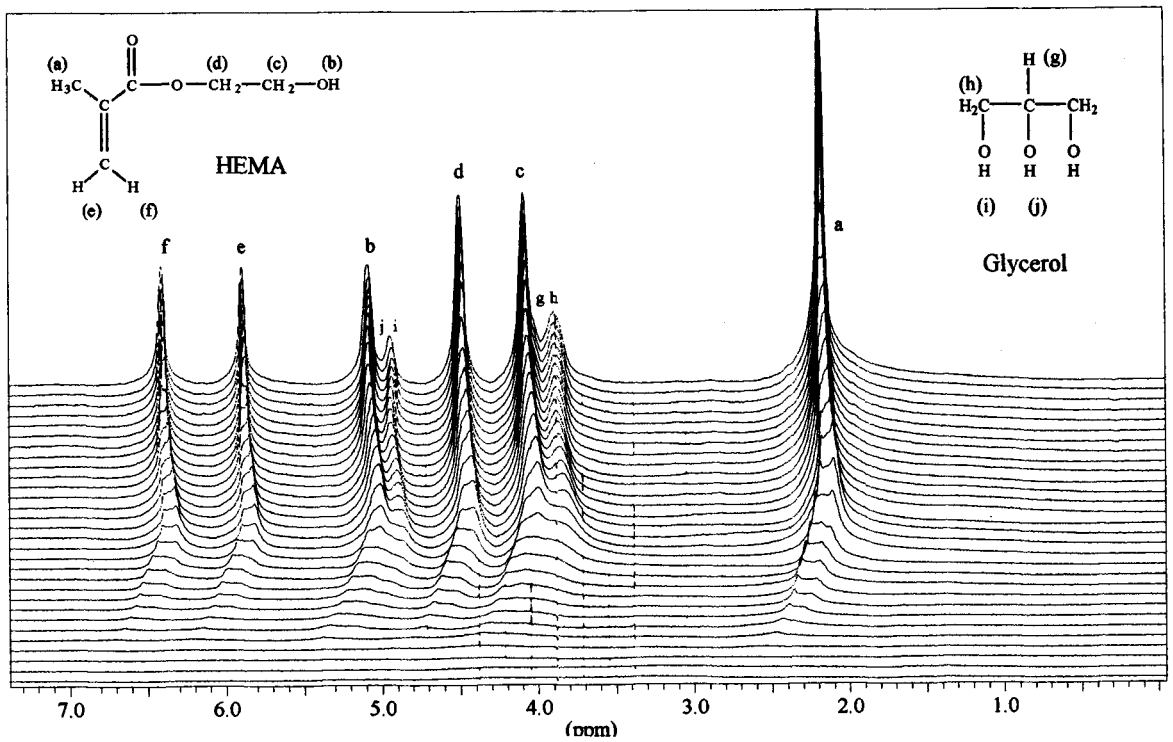

Figure 4. Overlaid ^{1}H NMR liquid spectra (293 K) from the UV-photoinitiated cure of sample A. Spectra were stored approximately every 30 s during the curing cycle.

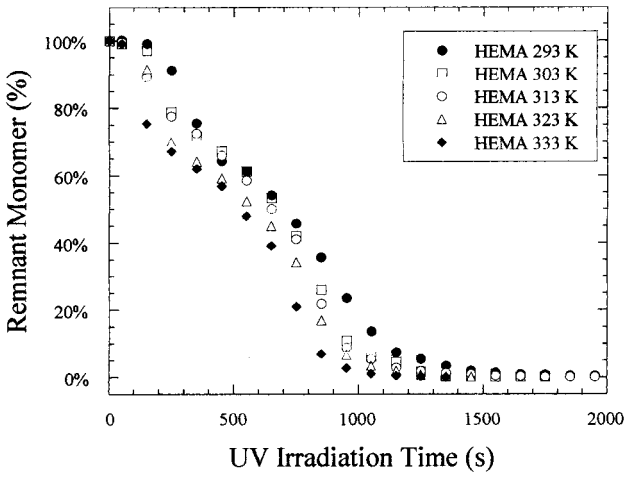

Figure 5. Curing profiles of sample A in the form of remnant monomer as a function of curing time determined from NMR spectra. Data were recorded for the range of temperatures indicated.

Comparison of NMR and FTIR Data. Casual inspection of Figures 2 and 7 reveals clear differences in the shape of the curing profiles of sample B as monitored by FTIR and NMR. Note initially that the time required to achieve a comparable conversion of monomer into polymer is about 1.25 times longer in the NMR experiments since the FTIR samples received ca. 1.6 times more UV light (0.048 mW cm^{-2}) than the NMR samples. Recall that the polymerization rate is proportional to the square root of the light intensity in the curing systems.[22]

Differences are most noticeable in the initial stages of cure; within the first ca. 1000 s, FTIR records a slow but progressive rate of cure in NVP whereas, in the case of NMR, the observed depletion of remnant liquid monomer is barely noticeable. Note also that the NMR chemical shifts of subpeaks decrease almost linearly while line width ΔB changes very little in this time regime (Figures 10−12).

FTIR monitors the depletion of C=C bonds via the progressive loss in intensity of the curing-sensitive bands listed in Table 1; this is the first step in the polymerization process. NMR line widths, on the other hand, discriminate between liquid monomer and solid polymer on the basis of their characteristic motional correlation frequencies relative to the bandwidth of the probe (ca. 4 kHz) which establishes the crossover frequency from liquid to solid in this experiment. Material with a correlation frequency greater than 4 kHz is deemed to be liquidlike (or a gel); a material with correlation frequencies lower than 4 kHz is considered to be solid polymer and no longer contributes to the observed spectral peak.

Chemical shifts of resonant nuclei are sensitive to their immediate environment and, in this respect, they more closely mimic the FTIR response. Thus, in the initial stage of curing both NMR chemical shifts and FTIR manifestly respond to the depletion of C=C bonds and the consequent formation of short oligomers which still retain a liquidlike mobility within the parameters of the NMR experiment, thereby leaving the NMR line widths and perceived remnant monomer levels reasonably invariant. This is in keeping with the observed behavior in Figures 2 and 7.

Summary

This paper reports on the use of high resolution NMR to profile the curing dynamics in real time in two monomers, one predominantly HEMA and the other a HEMA/NVP/TBE comonomer. FTIR data for the same samples demonstrate the complementarity of the two experimental techniques. Observed differences in the

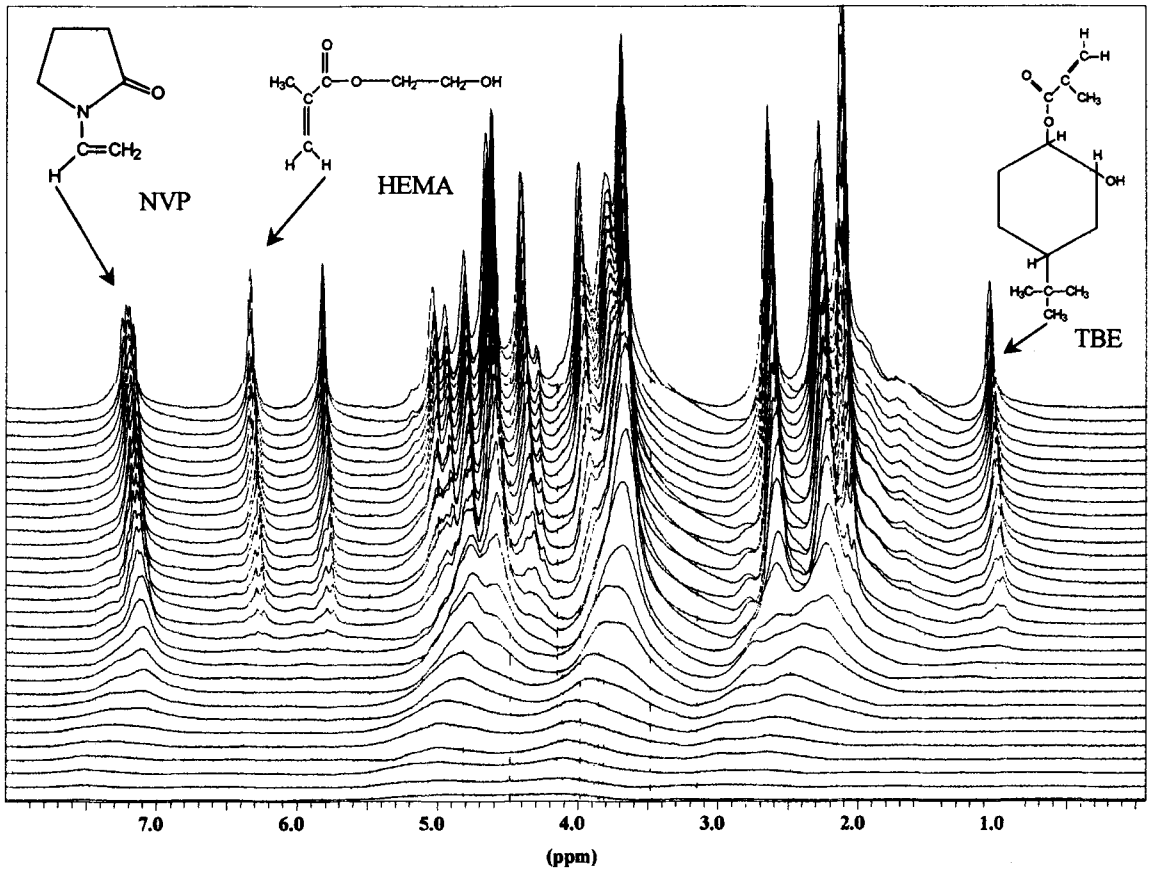

Figure 6. Overlaid ^{1}H NMR liquid spectra (293 K) from the UV-photoinitiated cure of sample B. Spectra were stored approximately every 30 s during the curing cycle.

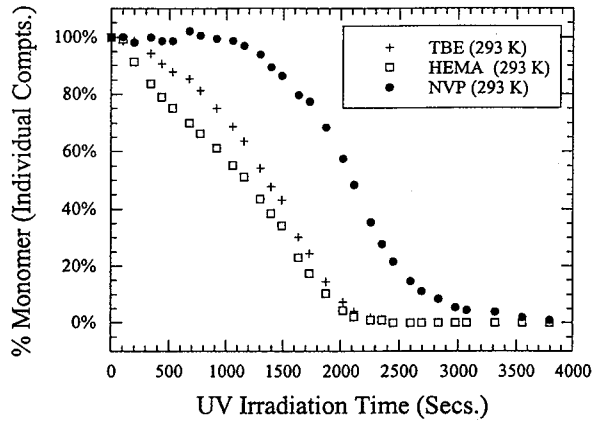

Figure 7. Curing profiles of the three constituent monomers in sample B as a function of curing time determined from NMR spectra (293 K).

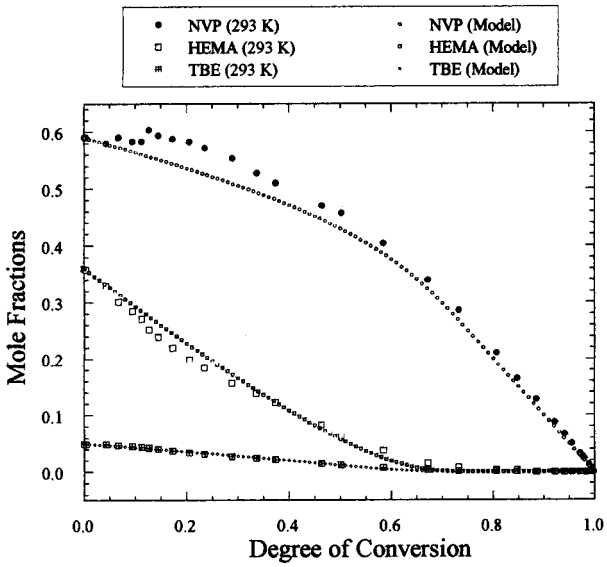

Figure 8. Mole fractions of the constituent monomers in sample B as a function of the instantaneous degree of conversion of copolymer. These data are compared with model simulations based on the $Q-e$ values listed in Table 2.

curing profiles generated in the two experimental approaches are rationalized in terms of their relative sensitivities to short and longer range effects in the curing monomer. The experimental responses are fitted to model simulations generated by a new numerical implementation which is applicable to an N-component monomer mix. The agreement based on published reactivity ratios for NVP and HEMA and those of a reasonable analogue for TBE is good.

While overall agreement between theory and experiment is satisfying, interpretation in some instances must be viewed as tentative pending further, more detailed, investigation. Two areas of study immediately come to mind. First, it would be interesting to quantify free radical concentrations, particularly in the initial stage of curing: electron spin resonance (ESR) or susceptibility measurements might accomplish this if the free radicals are sufficiently long-lived. Second, examination of possible differences between pulsed, synchronized irradiation and data acquisition, as op-

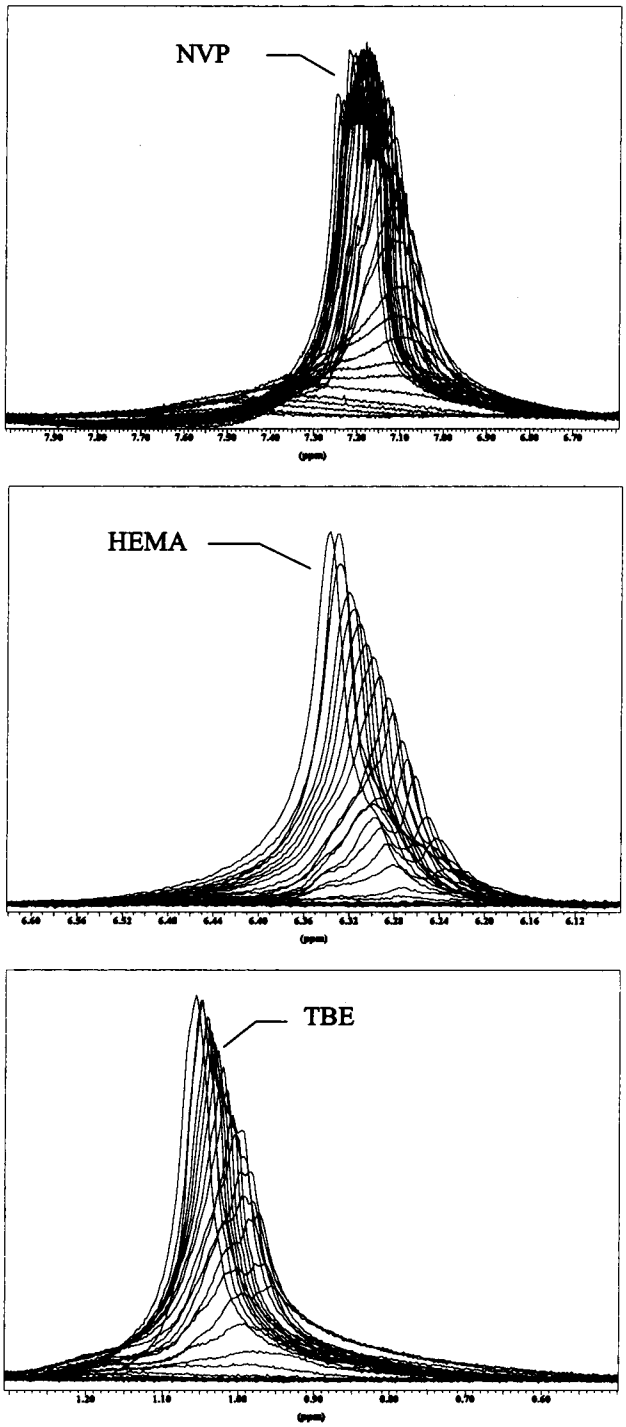

Figure 9. Superposition of the curing-sensitive spectral lines for NVP, HEMA and TBE in sample B (Figure 6) which illustrate the dependence of line shape and chemical shift on curing.

posed to continuous irradiation, may offer another avenue for probing the free radical activity.

Acknowledgment. It is a pleasure to acknowledge the continuing financial support of Bausch & Lomb during the course of this research.

Appendix

On the basis of the simplifying assumptions that free radical concentrations are always in a steady state, and that initial concentrations are such that all monomer concentrations are zero when reaction is complete, the

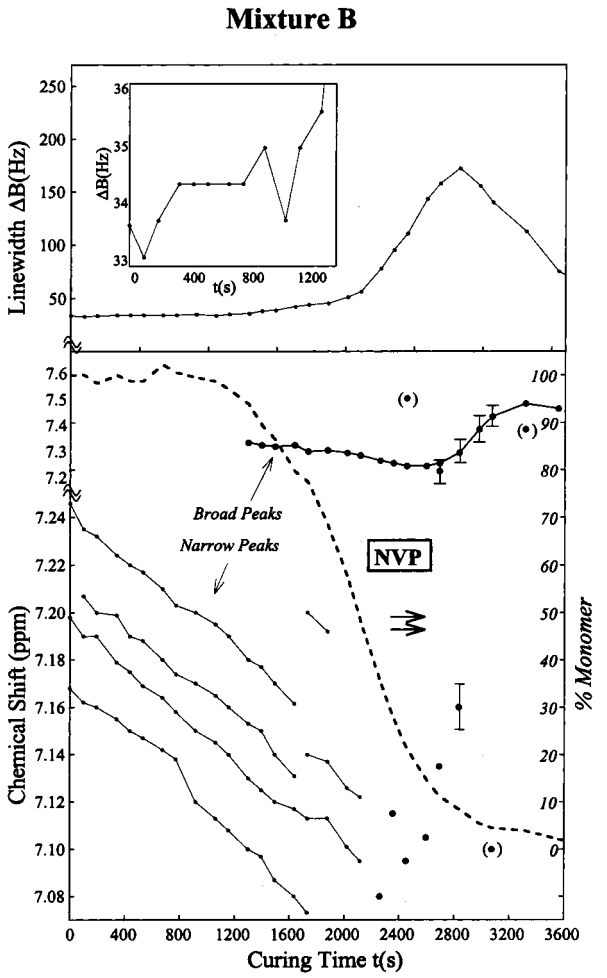

Figure 10. Dependence of chemical shifts of the resolved broad (●) and narrow (•) subpeaks on UV curing time for NVP in sample B (Figure 6). The curing profile (dashed line) is superimposed. The upper diagram shows the line width dependence on curing time and the insert shows the unusual line width behavior over the initial period of the curing cycle.

$Q-e$ scheme of parametrizing binary reaction rate kinetics leads to the following differential relations[1] for the mole fraction monomer concentrations:

$$\frac{\mathrm{d}[C_1]}{\mathrm{d}[C_i]} = \frac{[C_1]\sum_{k=1}^{n} d_{1k}[C_k]}{[C_i]\sum_{k=1}^{n} d_{ik}[C_k]}; \quad \{i = 2,3,..,n\}; \quad d_{ij} = Q_i Q_j \mathrm{e}^{-e_i e_j} \tag{1A}$$

The concentrations are to be obtained as functions of the degree of polymerization, θ, defined by

$$\theta = 1 - \sum_{i=1}^{n} [C_i]$$

Differential equations of the form,

$$\frac{\mathrm{d}[C_i]}{\mathrm{d}\theta} = -[C_i]F([\vec{C}])\sum_{k=1}^{n} d_{ik}[C_k]; \quad \{i = 1, 2, 3, ..., n\} \tag{2A}$$

imply the differential relations in eq 1A, and it is this representation of the problem that is used in the

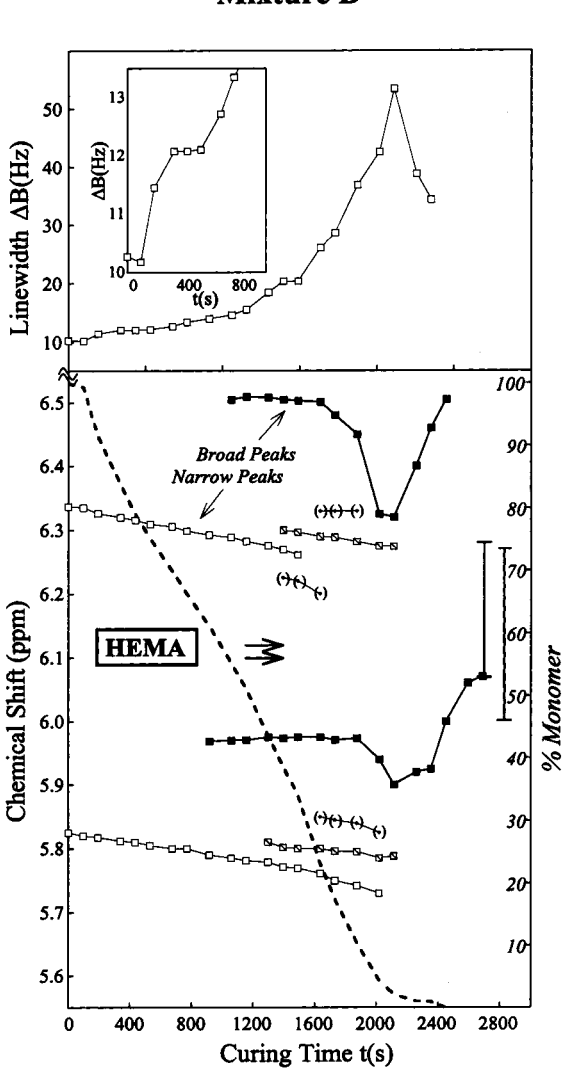

Figure 11. The dependence of chemical shifts of the resolved broad (■) and narrow (□) subpeaks on UV curing time for HEMA in sample B (Figure 6). The curing profile (dashed line) is superimposed. The upper diagram shows the line width dependence on curing time and the insert shows the unusual line width behavior over the initial period of the curing cycle. Chemical shift data are shown for both HEMA peaks in Figure 6.

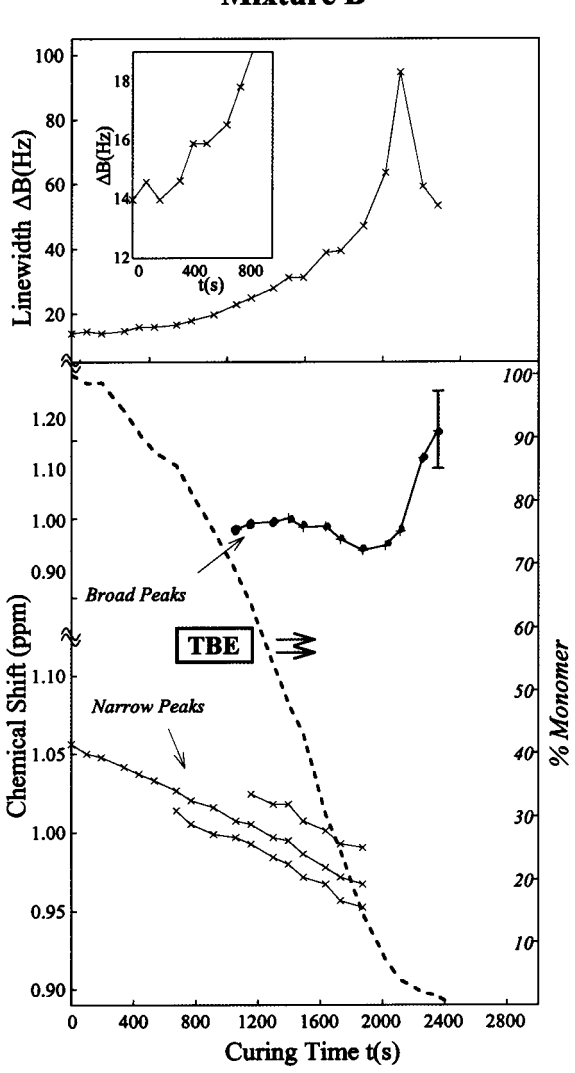

Figure 12. Dependence of chemical shifts of the resolved broad (●) and narrow (×) subpeaks on UV curing time for TBE in sample B (Figure 6). The curing profile (dashed line) is superimposed. The upper diagram shows the line width dependence on curing time and the insert shows the unusual line width behavior over the initial period of the curing cycle.

following. As suggested by eq 2A, θ is taken to be the independent variable. The definition of θ is used to eliminate one of the concentrations, which is taken to be $[C_1]$ without loss of generality. This change of variables gives

$$\frac{\mathrm{d}[C_i]}{\mathrm{d}\theta} = -[C_i]F([\vec{C}])((1-\theta)d_{i1} + \sum_{k=2}^{n}(d_{ik} - d_{i1})[C_k]); \quad \{i = 2,3,...,n\} \quad (3A)$$

for the remaining concentrations. The function $F(\vec{C})$ is determined by the requirement, from the definition of θ, that

$$-\sum_{i=1}^{n}\mathrm{d}[C_i]/\mathrm{d}\theta = F([\vec{C}])\sum_{i=1}^{n}\sum_{k=1}^{n}d_{ik}[\vec{C}_k] = 1 \quad (A4)$$

Elimination of $[C_1]$ from this relation gives an explicit expression for $F(\vec{C}) = F(x, C_2, ..., C_n)$,

$$-\sum_{i=1}^{n}\frac{\mathrm{d}[C_i]}{\mathrm{d}\theta} = F([\vec{C}])(d_{11}[C_1]^2 + 2[C_1]\sum_{k=2}^{n}d_{1k}[C_k] + \sum_{k=2}^{n}\sum_{i=2}^{n}[C_i]d_{ik}[C_k]) =$$

$$F([\vec{C}])\left(\begin{array}{l} d_{11}((1-\theta) - \sum_{k=2}^{n}[C_k])^2 + \\ ((1-\theta) - \sum_{k=2}^{n}[C_k])\sum_{k=2}^{n}d_{1k}[C_k] + \sum_{i,k=2}^{n}[C_i]d_{ik}[C_k] \end{array}\right) = 1 \quad (5A)$$

It is clearly a convenience to change the independent variable to $x = 1 - \theta$. These equations now have the form expected by standard algorithms for numerical solution of $(n - 1)$ coupled, first-order differential equations for $(n - 1)$ dependent variables, $[Ck]\{k = 2, ..., n\}$. The well-tested Runge−Kutta algorithm, for example, is quite stable in the presence of less than severe stiffness in these nonlinear equations, and is used in this work.[23]

References and Notes

(1) Valvassori, A.; Sartori, G. *Adv. Polym. Sci.* **1967**, *5*, 30.
(2) Koenig, J. L. Fourier Transform Infrared Spectroscopy of Polymers. *Adv. Polym. Sci.*, **1983**, *54*.
(3) Martin, S. J.; O'Brien, J. E.; Dowling, J.; McBrierty, V. J. *Eur. Polym. J.* **1998**, *34*, 1817.
(4) Quinn, F. X.; Kampff, E.; Smyth, G.; McBrierty, V. J. *Macromolecules* **1988**, *21*, 3191.
(5) Smyth, G.; Quinn, F. X.; McBrierty, V. J. *Macromolecules* **1988**, *21*, 3198.
(6) A preliminary report of our current research has been published in: Martin, S. J.; McBrierty, V. J.; Dowling, J.; Douglass, D. C. *Macromol. Rapid Commun.* **1999**, *20*, 95.
(7) Odian, G. *Principles of Polymerization*, 3rd ed.; J. Wiley and Sons: New York, 1991.
(8) Brandrup, J.; Immergut, E. H. *Polymer Handbook*, 3rd ed.; J. Wiley and Sons: New York, 1989.
(9) Fordyce, R. G.; Chapin, E. C.; Ham, G. E. *J. Am. Chem. Soc.* **1948**, *70*, 2489.
(10) McBrierty, V. J.; Magan, J.; Blau, W. Laser Curing of Contact Lens. European Patent No. 0447169, 1991.
(11) Mijovic, J.; Andjelic, S. *Polymer* **1995**, *36*, 3783.
(12) McBrierty, V. J.; Packer, K. J. *Nuclear Magnetic Resonance of Solid Polymers*; Cambridge University Press: Cambridge, U.K., 1993.
(13) Derome, A. *Modern NMR Techniques for Chemistry Research*; Pergamon Press: Oxford, U.K., 1991.
(14) Shaka, A. J.; Keeler, J.; Freeman, R. *J. Magn. Reson.* **1983**, *52*, 335: **1983**, *53*, 313.
(15) Walling, C.; Briggs, E. R. *J. Am. Chem. Soc.* **1945**, *67*, 1774.
(16) Alfrey, T., Jr.; Goldfinger, *J. Chem. Phys.* **1944**, *12*, 205.
(17) Alfrey, T., Jr.; Price, C. C. *J. Polym. Sci.* **1947**, *2*, 101.
(18) It is of interest to conjecture that the development of such stiffness would have corresponding physical analogues such as concentration or temperature sensitivity, or even instability, in the coploymerization process.
(19) Promath 2.0 Library, Copyright 1992−93 TeraTech, Inc., 100 Park Ave., Suite 360, Rockville, MD 20850: 1989 Hammerly Computer Services, Inc.
(20) Davis, T. P.; Huglin, M. B. *Macromolecules* **1989**, *22*, 2824. In this context it is noted that only those rates calculated at the beginning (or end) of the call to the integration algorithm should be saved, as opposed to the intermediate results in the algorithm.
(21) PowerBasic, Inc., 316 Mid Valley Center, Carmel, CA 93923.
(22) Rabek, J. F. Experimental and Analytical Methods for the Investigation of Radiation Curing. In *Radiation Curing in Polymer Science and Technology*; Fouassier, J. P., Rabek, J. F., Eds.; Elsevier Science: London, 1993. p 357.
(23) Further details of the program which is based on a modification of a standard commercially available Runge−Kutta package are available from the authors.

MA010645Z